CHAPTER 4
RECONSTRUCTION PROCEDURES

4.1 Introduction

The Fourier Diffraction Theorem as derived in Chapter 3 shows that when an object is illuminated with a plane wave traveling in the positive y-direction, the Fourier transform of the forward scattered fields gives values of the object's Fourier transform on an arc. Therefore, if an object is illuminated from many different directions it is possible, in principle, to fill up a disc of diameter $\sqrt{2}k$ in the frequency domain with samples of the Fourier transform of the object and then reconstruct the object by direct Fourier inversion. Therefore, diffraction tomography, using forward scattered data only, determines the object up to a maximum angular spatial frequency of $\sqrt{2}k$. To this extent, the reconstructed object is a low pass version of the original. In practice, the loss of resolution caused by this bandlimiting is negligible, being more influenced by considerations such as the aperture sizes of the transmitting and receiving elements, etc.

The fact that the frequency domain samples are available over circular arcs, whereas for convenient display it is desired to have samples over a rectangular lattice, is a source of computational difficulty in reconstruction algorithms for diffracting tomography. It should also be clear that by illuminating the object over 360°, a *double* coverage of the frequency domain is generated; note, however, that this double coverage is uniform. If the illumination is restricted to a portion of 360° there still will be a complete coverage of the frequency domain, however in that case there would be patches in the (ω_1,ω_2)-plane where there would be a double coverage. In reconstructing from circular arc grids to rectangular grids, it is often easier to contend with a uniform double coverage, as opposed to a coverage that is single in most areas and double in patches.

However, for some applications not given to data collection from all possible directions, it is useful to bear in mind that it is not necessary to go completely around an object to get complete coverage of the frequency domain. In principle, it should be possible to get an equal quality reconstruction when

illumination angles are restricted to a 180 ° plus interval, the angles in excess of 180 ° being required to complete the coverage of the frequency domain.

There are two computational strategies for reconstructing the object given measurements of the scattered field. As pointed out by [Sou84a] the two algorithms can be considered as interpolation in the frequency domain and in the space domain and are analogous to the direct Fourier inversion and backprojection algorithms of conventional tomography. Unlike conventional tomography, where backprojection is the preferred approach, the computational expense of space domain interpolation of diffracted projections makes frequency domain interpolation the preferred approach.

The remainder of this section will consist of derivations of the frequency domain and space domain interpolation algorithms. In both cases plane wave illumination will be assumed and the reader is referred to [Dev82, Pan83] for reconstruction algorithms for the synthetic aperture approach and to [Sou84b] for the general case.

4.2 Frequency Domain Interpolation

In order to discuss the frequency domain interpolation between a circular grid on which the data is generated by diffraction tomography, and a rectangular grid suitable for image reconstruction, parameters for representing each grid must be selected and then the relationship between the two sets of parameters written.

In Chapter 3, $U_B(\omega)$ was used to denote the Fourier transform of the transmitted data when an object is illuminated with a plane wave traveling along the positive y direction. Now $U_{B,\phi}(\omega)$ is used to denote this Fourier transform, where the subscript ϕ indicates the angle of illumination. This angle is measured as shown in Figure 4.1. Similarly, $Q(\omega,\phi)$ will be used to indicate the values of $o(\omega_1,\omega_2)$ along a semi-circular arc oriented at an angle ϕ as shown in Figure 4.2 or

$$Q(\omega,\sqrt{k_0^2-\omega^2}-k_0) \qquad |\omega| < k_0. \tag{4.1}$$

Therefore, when an illuminating plane wave is incident at angle ϕ, the equality

$$U_B(\alpha,l_0) = \frac{j}{2\sqrt{k_0^2-\alpha^2}} e^{j\sqrt{k_0^2-\alpha^2}l_0} O(\alpha,\sqrt{k_0^2-\alpha^2}-k_0) \tag{4.2}$$

can be rewritten as

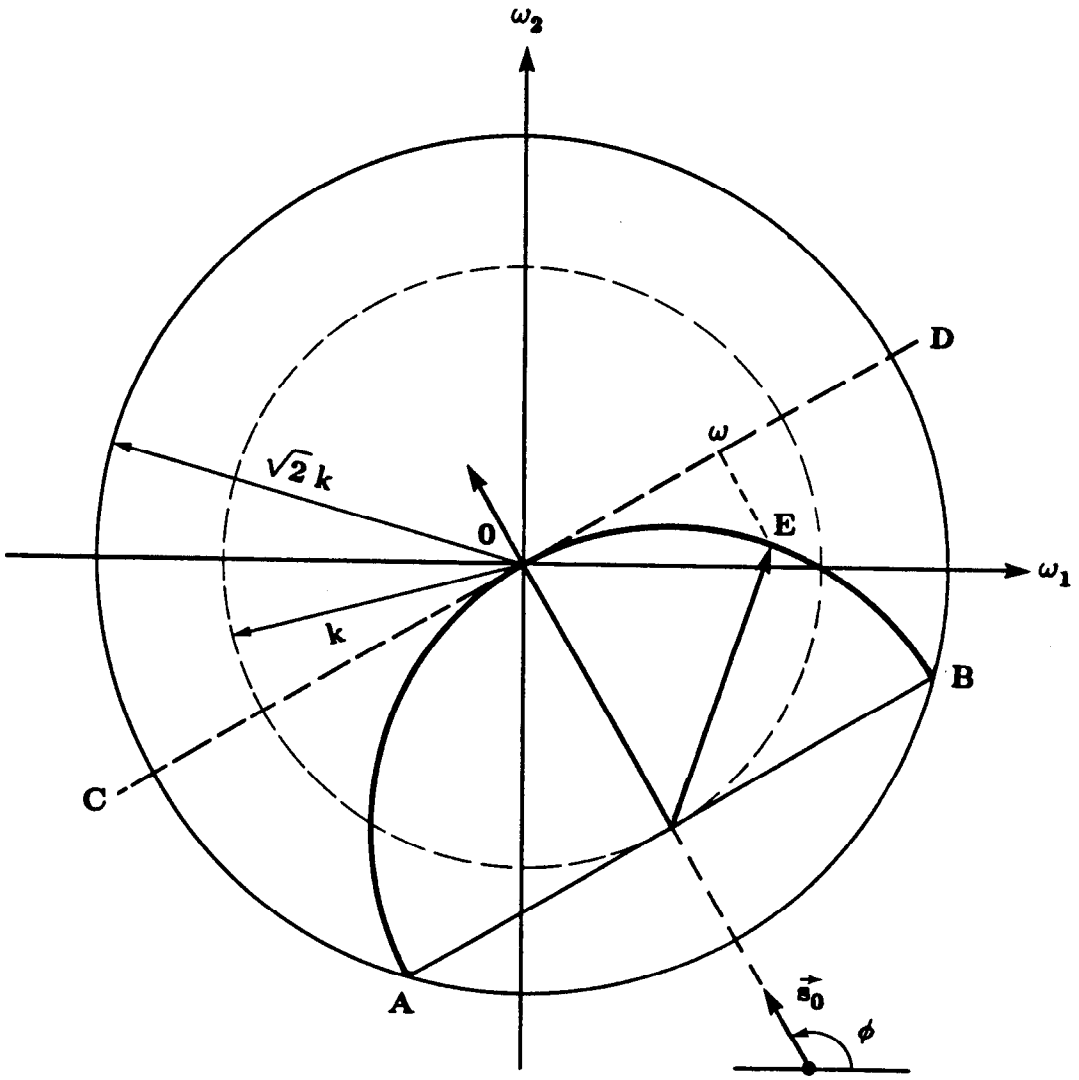

Figure 4.1 Each projection is measured using the phi–omega coordinate system shown here.

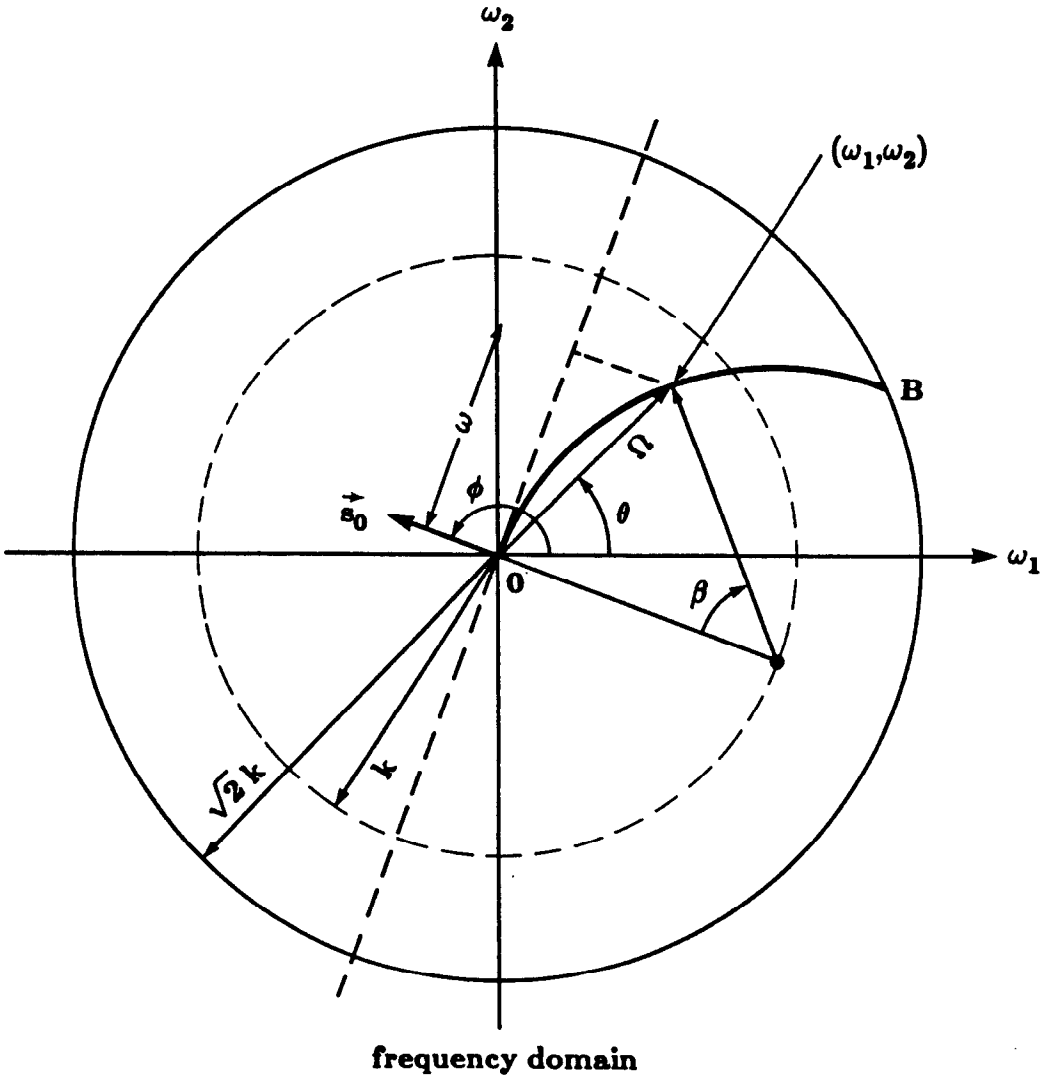

Figure 4.2 A second change of variables is used to relate the projection data to the object's Fourier transform.

$$u_{B,\phi}(\omega) = \frac{j}{2}\frac{1}{\sqrt{k^2-\omega^2}}\exp\left[j\ell\sqrt{k^2-\omega^2}\right]Q(\omega,\phi) \quad \text{for } |\omega| < k. \tag{4.3}$$

In most cases the transmitted data will be uniformly sampled in space, and a *discrete* Fourier transform of this data will generate uniformly spaced samples of $U_{B,\phi}(\omega)$ in the ω domain. Since $Q(\omega)$ is the Fourier transform of the object along the circular arc AOB in Figure 4.1 and since κ is the projection of a point on the circular arc on the tangent line CD, the uniform samples of Q in κ translate into non-uniform samples along the arc AOB as shown in Figure 4.3. For this reason designate each point on the arc AOB by its (ω,ϕ) parameters. [Note that (ω,ϕ) are *not* the polar coordinates of a point on arc AOB in Figure 4.2. Therefore, ω is *not* the radial distance in the (ω_1,ω_2) plane. For point E shown, the parameter ω is obtained by projecting E onto line CD.] The rectangular coordinates in the frequency domain will remain (ω_1,ω_2).

Before the relationships between (ω,ϕ) and (ω_1,ω_2), is presented it must be mentioned that the points generated by the AO and OB portions of the arc AOB must be considered separately as ϕ is varied from 0 to 2π. This is done because as mentioned before, the arc AOB generates a double coverage of the frequency domain, as ϕ is varied from 0 to 2π, which is undesirable for discussing a one-to-one transformation between the (ω,ϕ) parameters and the (ω_1,ω_2) coordinates.

Now reserve (ω,ϕ) parameters to denote the arc grid generated by one projection. It is important to note that for this arc grid, ω varies from 0 to k and ϕ from 0 to 2π.

The transformation equations between (ω,ϕ) and (ω_1,ω_2) will now be presented. This is accomplished in a slightly round-about manner by first defining polar coordinates (Ω,θ) in the (ω_1,ω_2)-plane as shown in Figure 4.2. In order to go from (ω_1,ω_2) to (ω,ϕ), first transform from the former coordinates to (Ω,θ) and then from (Ω,θ) to (ω,ϕ). The rectangular coordinates (ω_1,ω_2) are related to the polar coordinates (Ω,θ) by (Figure 4.2)

$$\Omega = \sqrt{\omega_1^2 + \omega_2^2} \tag{4.4}$$

$$\theta = \tan^{-1}\left[\frac{\omega_2}{\omega_1}\right]. \tag{4.5}$$

In order to relate (Ω,θ) to (ω,ϕ), a new angle β, which is the angular position of a point (ω_1,ω_2) on arc OB in Figure 4.2, is introduced. Note from the figure that the point characterized by angle β is also characterized by parameter ω.

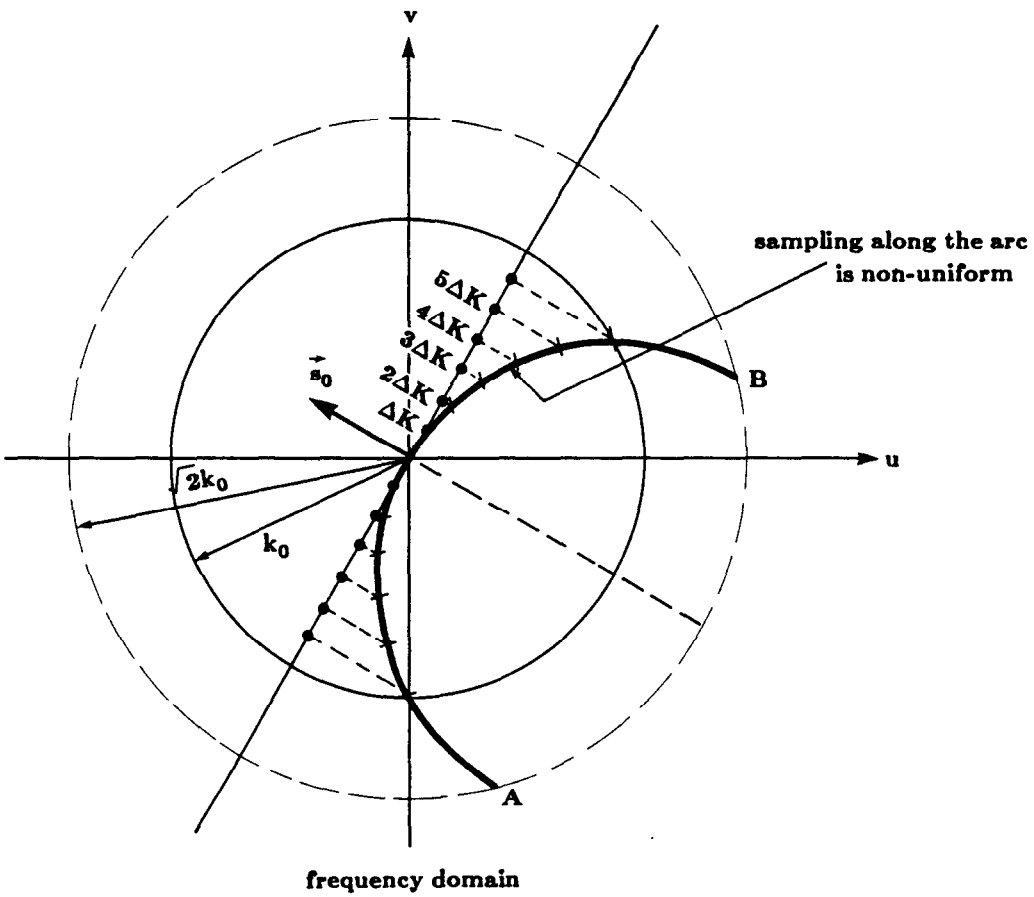

Figure 4.3 Uniformly sampling the projection in the space domain leads to uneven spacing of the samples of the Fourier transform of the object along the semi-circular arc.

The relationship between ω and β is given by

$$\omega = k \sin\beta. \tag{4.4}$$

The following relationship exists between the polar coordinates (Ω,θ) on the one hand and the parameters β and ϕ on the other:

$$\beta = 2\sin^{-1}\frac{\Omega}{2k} \tag{4.6}$$

$$\phi = \theta + \frac{\pi}{2} + \frac{\beta}{2}. \tag{4.7}$$

By substituting Equation (4.6) in (4.4) and then using (4.4), ω can be expressed in terms of ω_1 and ω_2. This result is shown below. Similarly, by substituting Equation (4.5) in (4.7), the following expression is obtained for ω and ϕ

$$\omega = \sin\left\{2\sin^{-1}\left(\frac{\sqrt{\omega_1^2 + \omega_2^2}}{2k}\right)\right\} \tag{4.8}$$

$$\phi = \tan^{-1}\left(\frac{\omega_2}{\omega_1}\right) + \sin^{-1}\left(\frac{\sqrt{\omega_1^2 + \omega_2^2}}{2k}\right) + \frac{\pi}{2}. \tag{4.9}$$

These are the transformation equations for interpolating from the (ω,ϕ) parameters used for data representation to the (ω_1,ω_2) parameters needed for inverse transformation.

To convert a particular rectangular point into (ω,ϕ) domain, substitute its ω_1 and ω_2 values in Equations. (4.8) and (4.9). The resulting values for ω and ϕ may not correspond to any for which $Q(\omega,\phi)$ is known. By virtue of equation (4.3), $Q(\omega,\phi)$ will only be known over a uniformly sampled set of values for ω and ϕ. In order to determine Q at the calculated ω and ϕ, the following procedure is used. Given $N_\omega \times N_\phi$ uniformly located samples, $Q(\omega_i,\phi_j)$, calculate a bilinearly interpolated value of this function at the desired ω and ϕ by using

$$Q(\omega,\phi) = \sum_{i=1}^{N_\omega}\sum_{j=1}^{N_\phi} Q(\omega_i,\phi_j)h_1(\omega-\omega_i)h_2(\phi-\phi_j), \tag{4.10}$$

where

$$h_1(\omega) = \begin{cases} 1-\dfrac{|\omega|}{\Delta\omega} & 0 \\ |\omega| \le \Delta\omega & \text{otherwise,} \end{cases} \tag{4.11}$$

$$h_2(\phi) = \begin{cases} 1-\dfrac{|\phi|}{\Delta\phi} & 0 \\ |\phi| \leq \Delta\phi & \text{otherwise;} \end{cases} \qquad (4.12)$$

$\Delta\phi$ and $\Delta\omega$ are the sampling intervals for ϕ and ω, respectively. When expressed in the manner shown above, bilinear interpolation may be interpreted as the output of a filter whose impulse response is $h_1 h_2$.

The results obtained with bilinear interpolation can be considerably improved if the sampling density in the (ω,ϕ)-plane is increased by using the computationally efficient method of zero-extending the inverse two-dimensional inverse *Fast Fourier Transform* (FFT) of the $Q(\omega_i,\phi_j)$ matrix. The technique consists of first taking a two-dimensional inverse FFT of the $N_\omega \times N_\phi$ matrix consisting of the $Q(\omega_i,\phi_j)$ values, zero-extending the resulting $N_\omega \times N_\phi$ array of numbers to, perhaps, $mN_\omega \times nM_\phi$ and then taking the FFT of this new array. The result is an mn-fold increase in the density of samples in the (ω,ϕ)-plane. After computing $Q(\omega,\phi)$ at each point of a rectangular grid by the procedure outlined above, the object f(x,y) is obtained by a simple 2-D inverse FFT.

The use of bilinear interpolation and zero padding are both good techniques for resampling a function but they are used here in a non standard way. Typically interpolation algorithms are derived assuming that the sampled data can be described as nearly linear (when using bilinear interpolation) and frequency limited (when using Fourier domain zero padding) [Con80, Sto80, Act70]. In this application, when resampling the data from a circular grid to a rectangular grid, the function is assumed to be smooth in the Fourier domain. This assumption is reasonable since the data is assumed to be well behaved.

The interpolation described above, however, is carried out in a rectilinear version of the (ω,ϕ) coordinate system. Thus four points in the (ω,ϕ) space, where data is available, are first assumed to be at the four corners of a rectangle and then the interpolation is calculated for a point in the middle. This is an approximation because the four data points actually define a smooth function that is defined along four points on two of the circular arcs. As will be seen in the reconstructions the effect of this approximation is small but it should be remembered when comparing interpolation schemes.

4.3 Backpropagation Algorithms

It has recently been shown by Devaney [Dev82] and Kaveh [Kav82] that there is an alternative method for reconstructing images from the diffracted projection data. This procedure, called the *filtered-backpropagation method*, is similar in spirit to the filtered-backprojection techniques which (due to their superior numerical accuracy) have been one factor in the enormous success of x-ray tomography. Unfortunately, whereas the filtered-backprojection algorithms also possess efficient implementations, the same cannot be said for the filtered-backpropagation algorithms. The latter class of algorithms is computationally intensive, much more so than the interpolation procedure discussed above. With regard to accuracy, they do not seem to possess any advantage especially if interpolation is carried out after increasing the sampling density by appropriate zero-padding as discussed above.

The derivation of the backpropagation algorithm will follow as presented by Devaney [Dev82]. First consider the inverse Fourier transform of the object function,

$$o(rv) = \frac{1}{(2\pi)^2} \int_{-\infty}^{\infty}\int_{-\infty}^{\infty} O(\vec{K})e^{j\vec{K}\cdot rv}d\vec{K}. \tag{4.13}$$

This integral represents the object function in terms of the Fourier transform of the object along a rectangular grid. As already discussed, a diffraction tomography experiment measures the Fourier transform of the object along circular arcs; thus it will be easier to perform the integration if it is modified to use the projection data more naturally. This will be done using two coordinate transformations: the first one will exchange the rectangular grid for a set of semicircular arcs and the second will map the arcs into their plane wave decomposition.

First exchange the rectangular grid for semi-circular arcs. To do this represent $\vec{K}=(k_x,k_y)$ in equation (4.13) by the vector sum

$$\vec{K} = k_0(\vec{s}-\vec{s}_0) \tag{4.14}$$

where $\vec{s}_0=(\cos\phi_0,\sin\phi_0)$ and $\vec{s}=(\cos\chi,\sin\chi)$ are unit vectors representing the direction of the wavevector for the transmitted and the received plane waves respectively. This coordinate transformation is illustrated in figure 4.4.

To find the Jacobian of this transformation write

$$k_x = k_0(\cos\chi-\cos\phi_0) \tag{4.15}$$

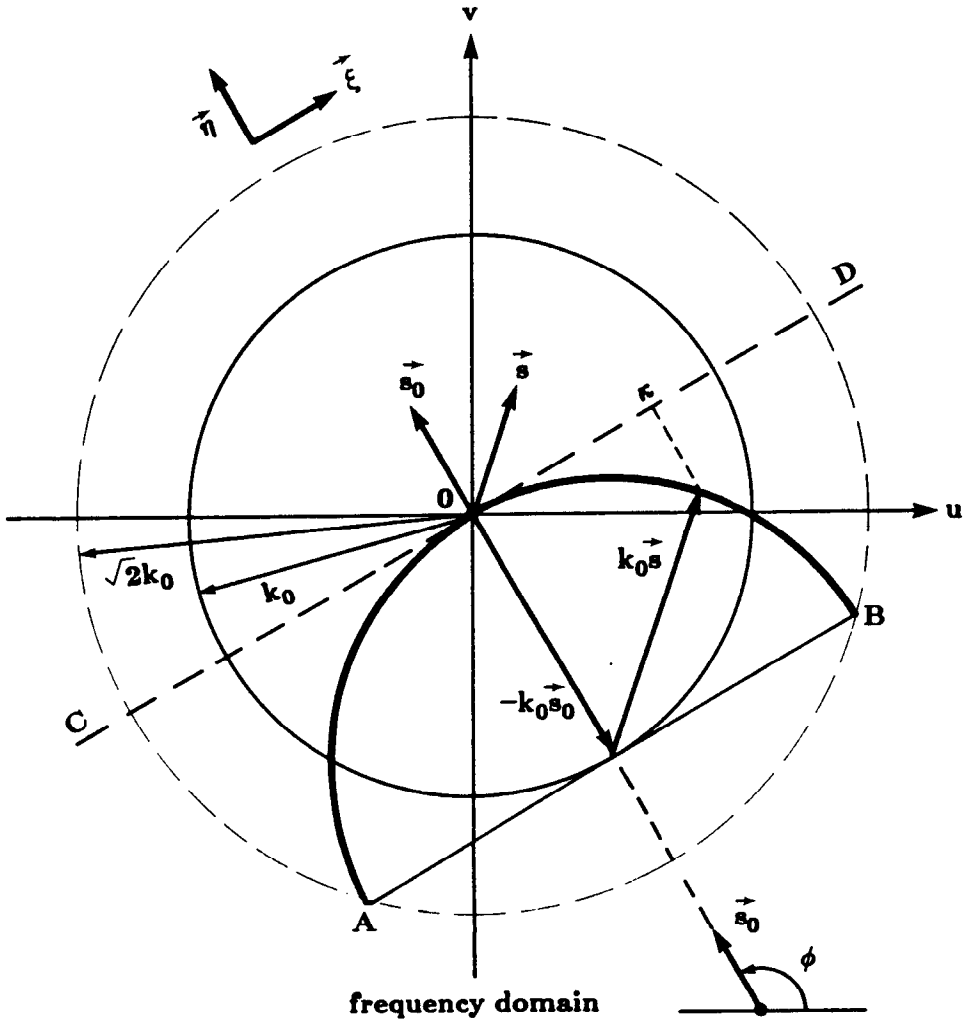

Figure 4.4 The $k_0\vec{s}_0$ and $k\vec{s}_0$ used in the backpropagation algorithm are shown here.

$$k_y = k_0(\sin\chi - \sin\phi_0) \tag{4.16}$$

and

$$dk_x dk_y = \left| k_0^2 \sin(\chi-\phi_0) \right| d\chi d\phi_0 \tag{4.17}$$

$$= k_0\sqrt{1-\cos^2(\chi-\phi_0)}\,d\chi d\phi_0 \tag{4.18}$$

$$= k_0\sqrt{1-(\vec{s}\cdot\vec{s}_0)^2}\,d\chi d\phi_0 \tag{4.19}$$

and then equation (4.13) becomes

$$o(rv) = \frac{1}{(2\pi)^2}\left(\frac{1}{2}\right)k_0^2 \int_0^{2\pi}\int_0^{2\pi} \sqrt{1-(\vec{s}\cdot\vec{s}_0)^2}\, O\left[k_o(\vec{s}-\vec{s}_0)\right] e^{jk_0(\vec{s}-\vec{s}_0)\cdot rv}\, d\chi d\phi_0. \tag{4.20}$$

The factor of $\frac{1}{2}$ is necessary because as discussed in section 4.2 the (χ,ϕ_0) coordinate system gives a double coverage of the (k_x,k_y) space.

This integral gives an expression for the scattered field as a function of the (χ,ϕ_0) coordinate system. While the data that is collected will actually be a function of ϕ_0, the projection angle, and κ, the one dimensional frequency of the scattered field along the receiver line. To make the final coordinate transformation take the angle χ to be relative to the (κ,γ) coordinate system diagramed in Figure 4.4. This is a more natural representation since the data available in a diffraction tomography experiment lies on a semicircle and therefore the data is available only for $0 \le \chi \le \pi$. The χ integral in equation (4.20) above can be rewritten by noting

$$\cos\chi = \kappa/k_0 \tag{4.21}$$

$$\sin\chi = \gamma/k_0 \tag{4.22}$$

and therefore

$$d\chi = \frac{-1}{k_0\gamma} d\kappa. \tag{4.23}$$

The χ integral becomes

$$\frac{1}{k_0}\int_{-k_0}^{k_0} \frac{d\kappa}{\gamma} \left|\kappa\right| O\left[k_0(\vec{s}-\vec{s}_0)\right] e^{jk(\vec{s}-\vec{s}_0)\cdot rv}\, d\kappa. \tag{4.24}$$

Using the Fourier Diffraction Theorem as represented by equation (4.2) the Fourier transform of the object function, O, can be approximated by a simple function of the first order Born field, u_B, at the receiver line. Thus the object

function in equation (4.24) can be written

$$O\left[k_0(\vec{s}-\vec{s}_0)\right] = -2\gamma j U_B(\kappa,\gamma-k_0)e^{-j\gamma l_0}. \tag{4.25}$$

In addition if a rotated coordinate system is used for $r = (\xi,\eta)$ where

$$\xi = x\sin\phi - y\cos\phi \tag{4.26}$$

and

$$\eta = x\cos\phi + y\sin\phi \tag{4.27}$$

then the dot product $k_0(\vec{s}-\vec{s}_0)$ can be written

$$\kappa\xi+(\gamma-k_0)\eta. \tag{4.28}$$

The coordinates (ξ,η) are illustrated in Figure 4.5. Using the results above the χ integral is now written as

$$\frac{2j}{k_0}\int_{-k_0}^{k_0} d\kappa\,|\kappa|\,U_B(\kappa,\gamma-k_0)e^{-j\gamma l_0}e^{\kappa\xi+(\gamma-k_0)\eta} \tag{4.29}$$

and the equation for the object function in equation (4.20) becomes

$$o(rv) = \frac{jk_0}{(2\pi)^2}\int_0^{2\pi} d\phi_0 \int_{-k_0}^{k_0} d\kappa\,|\kappa|\,U_B(\kappa,\gamma-k_0)e^{-j\gamma l_0}e^{j\kappa\xi+j(\gamma-k_0)\eta}. \tag{4.30}$$

To bring out the filtered-backpropagation implementation, the inner integration is written here separately:

$$\Pi_\phi(\xi,\eta) = \frac{1}{2\pi}\int_{-\infty}^{\infty} \Gamma_\phi(\omega)H(\omega)G_\eta(\omega)\exp(j\omega\xi)\,d\omega \tag{4.31}$$

where

$$\begin{aligned} H(\omega) &= |\omega|, && |\omega| \le k_0 \\ &= 0, && |\omega| > k_0 \\ G_\eta(\omega) &= \exp\left[j(\sqrt{k_0^2-\omega^2}-k_0)\right], && |\omega| \le k_0 \\ &= 0, && |\omega| > k_0 \end{aligned} \tag{4.32}$$

and

$$\Gamma_\phi(\omega) = U_B(\kappa,\gamma-k_0)e^{-j\gamma l_0}. \tag{4.33}$$

Without the extra filter function $G_\eta(\omega)$, the rest of Equation (4.31) would correspond to the filtering operation of the projection data in x-ray tomography. The filtering as called for by the transfer function $G_\eta(\omega)$ is depth

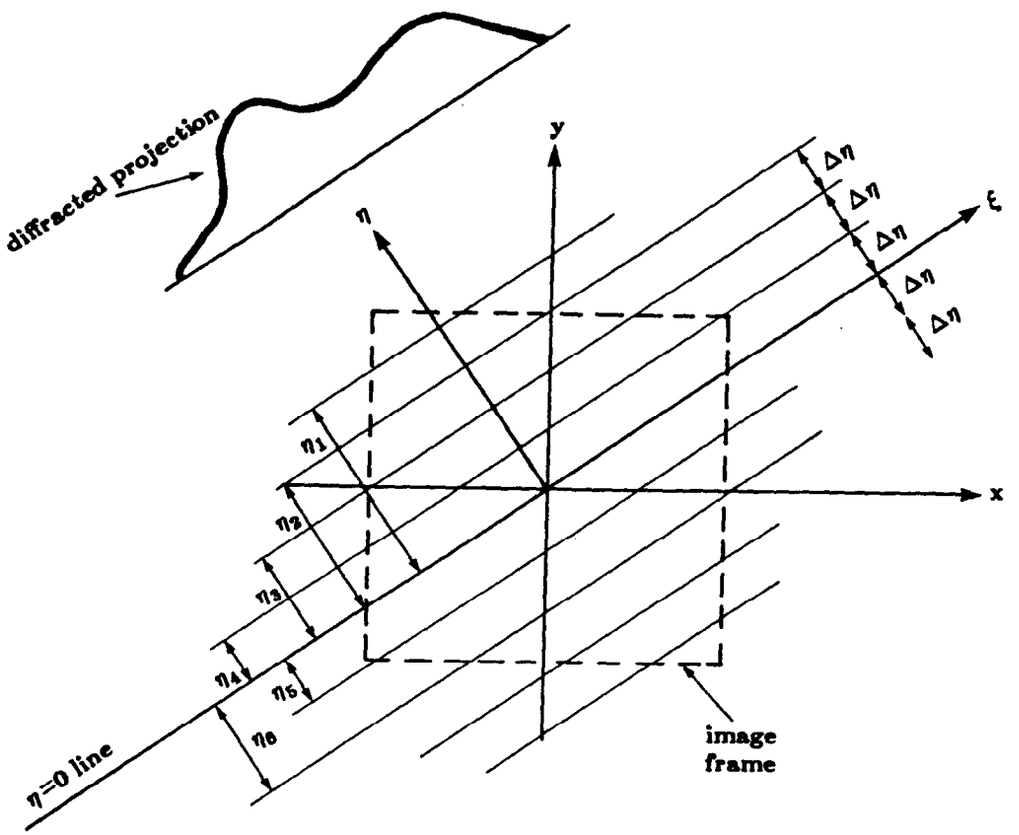

Figure 4.5 In backpropagation the project is backprojected with a depth dependent filter function. At each depth, η, the filter corresponds to propagating the field at a distance of $\Delta\eta$.

dependent due to the parameter η, which is equal to $x\cos\phi + y\sin\phi$.

In terms of the filtered projections $\Pi_\phi(\xi,\eta)$ in Equation (4.31), the reconstruction integral of Equation (4.30) may be expressed as

$$f(x,y) = \frac{1}{2\pi} \int_0^{2\pi} d\phi \, \Pi_\phi(x\sin\phi - y\cos\phi \, , \, x\cos\phi + y\sin\phi) \qquad (4.34)$$

The computational procedure for reconstructing an image on the basis of Equations (4.31) and (4.34) may be presented in the form of the following steps:

STEP 1: In accordance with Equation (4.31), filter each projection with a separate filter for each depth in the image frame. For example, if only 9 depths are used as shown in Figure 4.5, 9 different filters would need to be applied to the diffracted projection shown there. [In most cases for 128 x 128 reconstructive, the number of discrete depths chosen for filtering the projection will also be around 128. If there are much less than 128, spatial resolution will be lost.] [Cra79]

STEP 2: To each pixel (x,y) in the image frame, in accordance with Equation (4.34) allocate a value of the filtered projection that corresponds to the nearest depth line.

STEP 3: Repeat the preceding 2 steps for all projections. As a new projection is taken up, add its contribution to the current sum at pixel (x,y).

The depth dependent filtering in Step 1 makes this algorithm computationally very demanding. For example, if N_η depth values are used, the processing of each projection will take $(N_\eta+1)$ Fast Fourier Transforms (FFT's). If the total number of projections is N_ϕ, this translates into $(N_\eta+1)N_\phi$ FFT's. For most N x N reconstructions, both N_η and N_ϕ will be approximately equal to N. Therefore, the filtered-backpropagation algorithm will require approximately N^2 FFT's compared to 4N FFT's for bilinear interpolation. [For precise comparisons, it must be mentioned that the FFT's for the case of bilinear interpolation are longer due to zero-padding.]

Devaney [Dev82] has also proposed a modified filtered-backpropagation algorithm, in which $G_\eta(\omega)$ is simply replaced by a single $G_{\eta_0}(\omega)$ where $\eta_0 = x_0\cos\phi + y_0\sin\phi$, (x_0,y_0) being the coordinates of the point where local accuracy in reconstruction is desired. [Elimination of depth dependent filtering reduces the number of FFT's to $2N_\phi$.]

4.4 Signal Processing Concerns

The reconstruction algorithms described above and in [Pan83] involve a number of signal processing steps. The following work describes the quality of the final reconstruction when small changes are made to the signal processing procedure. These changes are valid for reconstruction algorithms using either space (backpropagation) or frequency domain interpolation.

Assuming first order approximations are valid, the algorithm for reconstructing an object from diffracted projections is briefly as follows:

1) Collect the data
2) Fourier Transform each projection
3) Estimate the 2-dimensional Fourier transform of the object from the transformed projections
4) Perform a 2-dimensional inverse Fourier transform to get an estimate of the object.

At each step of this procedure signal processing theory suggests a number of procedures to improve the reconstruction. These include

a) Zero padding the projection data to reduce the effects of interperiod interference. This also increases the resolution in the frequency domain and should make interpolation easier.
b) Applying a Hamming window to the projection data to smooth out the data at the ends of the receiver.
c) Multiplying the two dimensional Fourier Transform of the object by a Low Pass Filter (LPF) (a Hamming window in this case) to reduce the effects of high frequency noise.

These new steps are illustrated in Figure 4.6 where optional steps have been indicated with dashed boxes. we have indicated the optional steps with dashed boxes.

To evaluate the effects of each of these changes Figure 4.7 and Figure 4.8 shows the center line of reconstructions using all eight possible combinations of options. The data was generated for a cylinder of radius 1λ and a refractive index change of .5%.

An important part of the reconstruction process is filtering the projection data. For efficiency reasons the filter is implemented with an FFT algorithm but these algorithms do not perform an aperiodic convolution like that used in linear systems theory. Instead a filter implemented with FFT's performs circular convolution.

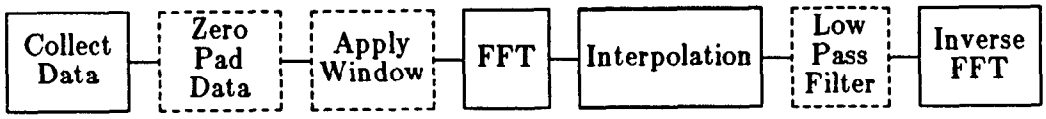

Figure 4.6 The signal processing steps in a typical diffraction tomography algorithm are shown here. The steps that are needed are shown with a solid box while the optional steps are shown with dashed lines.

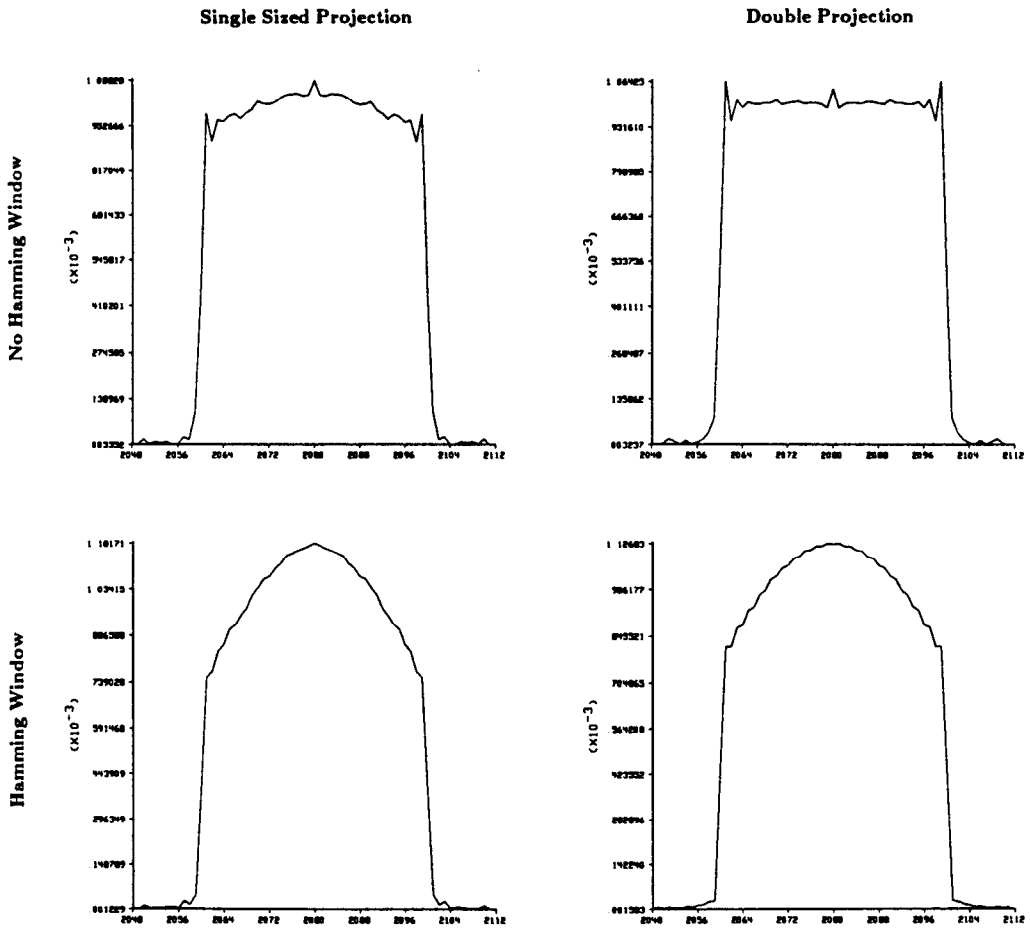

Figure 4.7 The center line of reconstructions are shown here with the size of the projection doubled and the Hamming window added. All reconstruction shown here are without low pass filtering.

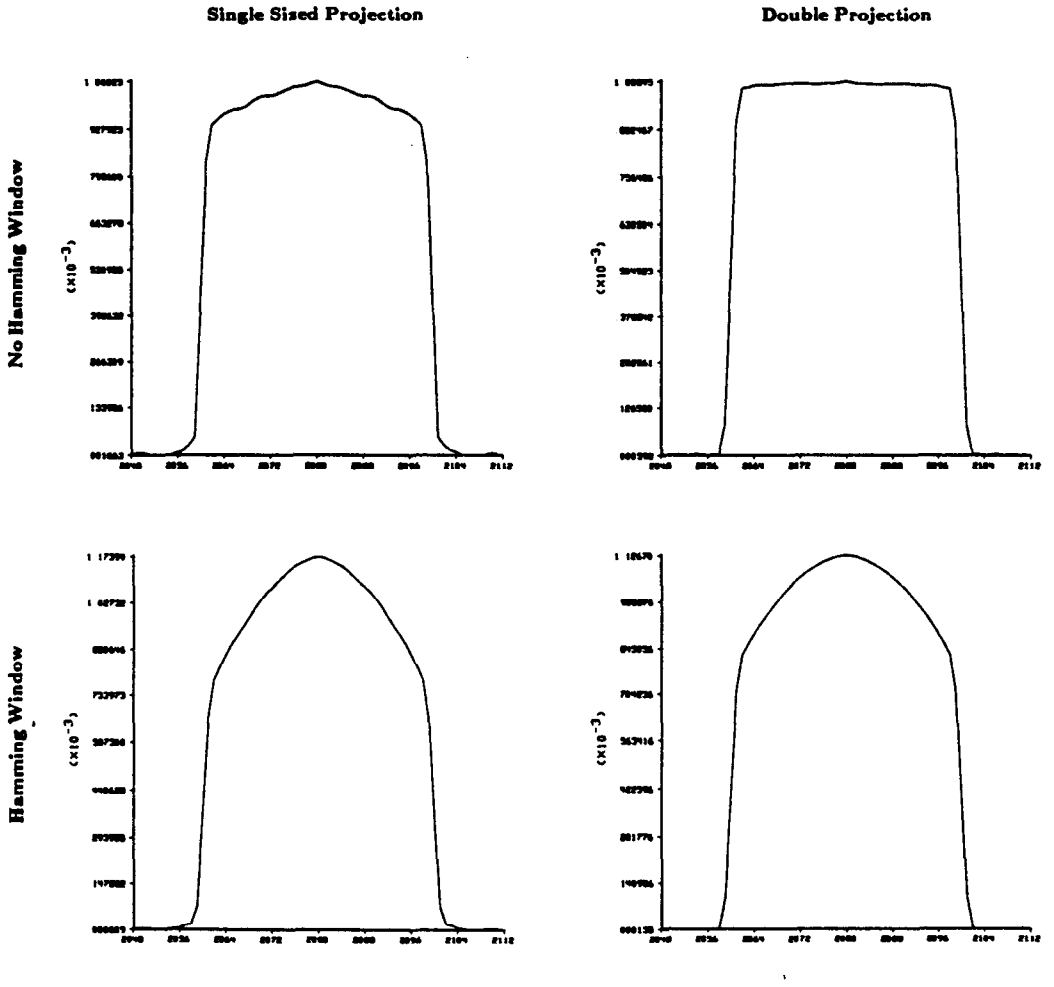

Figure 4.8 The center line of reconstructions are shown here with the size of the projection doubled and the Hamming window added. All reconstruction shown here are with low pass filtering.

If the data is first padded with zeros so that the new data sequence is twice as long as the original then the results produced by circular and aperiodic convolution are the same. In addition, zero padding the original projection increases the resolution of the data in the frequency domain and thus makes a simple interpolation scheme more accurate. Unfortunately the extra data more than doubles the computational time. (For example an FFT takes NlogN operations so when N is doubled the computational expense goes up by a factor of

$$\frac{(2N)\log_2(2N)}{N\log_2 N} = 2\left[1+\frac{2}{\log_2 N}\right] \tag{4.35}$$

Based on the reconstructions shown in Figure 4.7 it is possible to conclude that doubling the size of the projection data only makes a small improvement in the quality of the reconstructions. Since the extra zeros more than double the computational expense involved in filtering the data it is probably best not to zero pad.

A second signal processing concern is due to data truncation. In a real world experiment it is only possible to collect and process a finite amount of data. Generally this isn't a problem since the data eventually goes to zero outside of some range and the data can be truncated without loss of information. This is certainly true, for example, in x-ray CT projections but is not true with diffracted projections. With fields the amplitude decays proportional to $\frac{1}{R}$ and consequently the projection data never goes to zero.

Mathematically the data truncation error can be modeled as a multiplication in the space domain by a rectangular window [Opp75]. In the frequency domain this is equivalent to convolving the data with a sinc function and thus smoothes the frequency domain signal. A number of windows like the Hamming window have been designed to reduce the effects of data truncation.

Figure 4.7 shows that a Hamming window does not have the same positive effect with diffracted projections. In this case most of the high frequency information is at either end of the projection and thus the window only serves to attenuate the high frequency components. This is shown in Figure 4.9 where the Fourier transform of the diffracted projection is shown before (top graph) and after (bottom graph) applying a Hamming window to the projection data. The loss of high frequency data caused by the Hamming window leads to the rounded edges shown in the reconstructions shown in Figure 4.7.

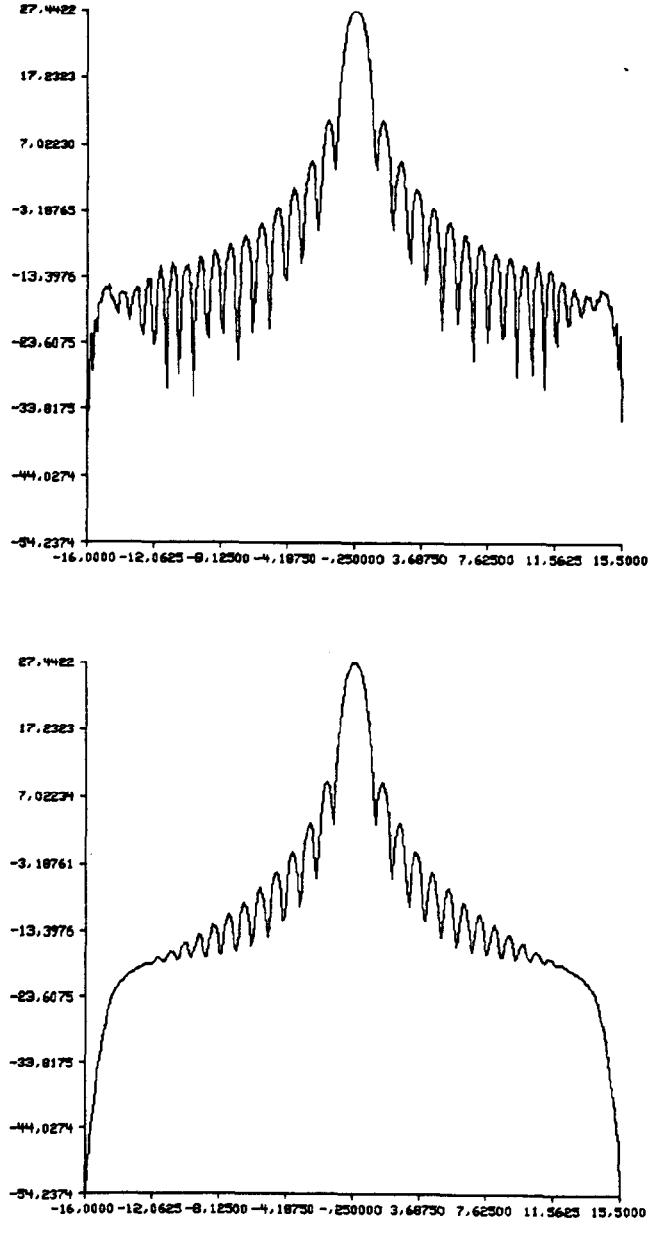

Figure 4.9 The spectrum of the field before (top graph) and after (bottom graph) multiplying by a Hamming window in the space domain are shown here.

Finally a very large improvement is observed by adding a Low Pass Filter before inverse Fourier transforming the data. The filtering done before interpolation includes a 1/k term which also serves to enhance the high frequency noise. By adding a LPF this effect is counteracted.

The best results would be obtained if it would be possible to characterize the spectral density of the signal and the noise and then design a Wiener filter. This is a difficult problem and adequate results were obtained by using a Low Pass Filter of the form

$$w(\omega) = 0.54 + 0.46\cos(\frac{\omega T}{2}) \tag{4.36}$$

Based on the results shown in Figure 4.7 and 4.8 the best reconstructions are obtained if a low pass filter is used to smooth the final reconstruction but that zero padding the projection data and applying a Hamming window to the projection data do not improve the results.

Finally a small improvement was made to the backpropagation algorithm by using bilinear interpolation instead of nearest neighbor. The backpropagation algorithm consists of both a depth dependent filter and then the addition to each pixel of a portion of the backpropagated field. In the original formulation each pixel is assigned the nearest neighbor in the field, but as shown in Figure 4.10 even better results are obtained if the valued added to each pixel is calculated using bilinear interpolation. Compared to the expense of doing the backpropagation filter the bilinear interpolation cost is inconsequential and thus worth the effort.

This is also shown when the Mean Squared Error in the reconstructions is computed. The table below compares the error for bilinear interpolation versus nearest neighbor and bilinear backpropagation. As can be seen from Table 4.1, bilinear interpolation significantly improves the reconstruction.

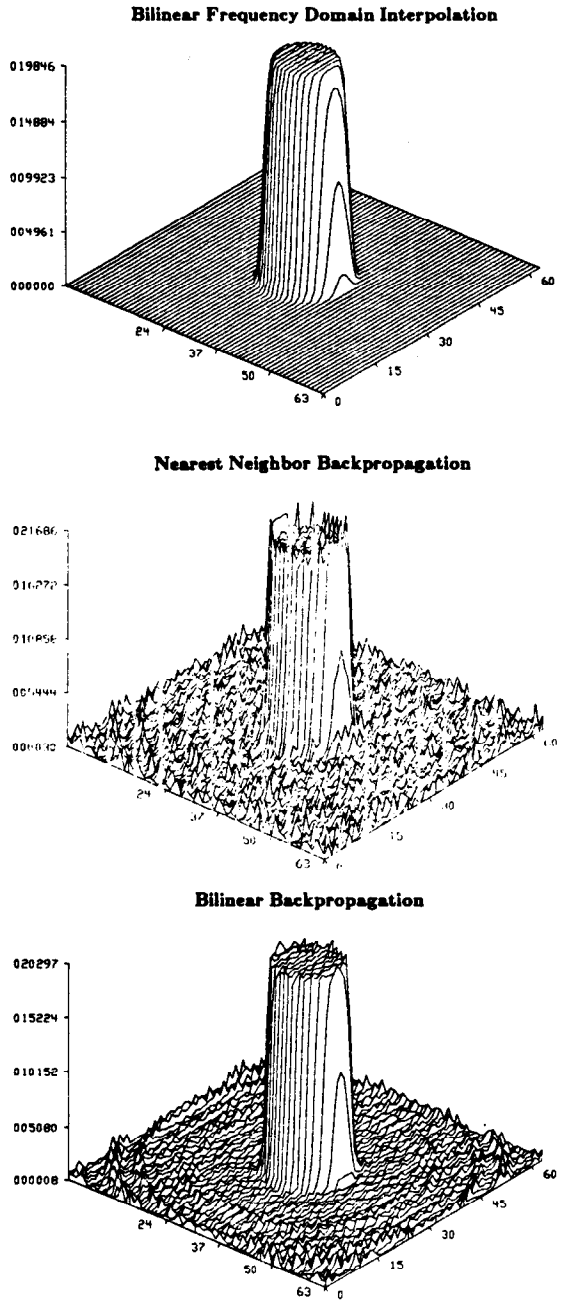

Figure 4.10 Reconstructions of a cylinder are shown comparing nearest neighbor and bilinear interpolation for frequency domain and space domain reconstruction algorithms.

Table 4.1. Mean Squared Error in a reconstruction of a cylinder using three interpolation schemes.

Mean Squared Error	
Bilinear Interpolation	4.8%
Nearest Neighbor Backpropagation	6.8%
Bilinear Backpropagation	4.8%

References

[Act70] F. S. Acton, *Numerical Methods that Work,* Harper & Row, New York, 1970.

[Con80] S. D. Conte and C. deBoor, *Elementary Numerical Analysis,* McGraw-Hill, New York, 1980.

[Cra79] C. R. Crawford and A. C. Kak, "Aliasing artifacts in computerized tomography," *Appl. Opt.*, Vol. 18, 1979, pp. 3704-3711.

[Dev82] A. J. Devaney, "A filtered backpropagation algorithm for diffraction tomography," *Ultrasonic Imaging,* Vol. 4, 1982, pp. 336-350.

[Kav82] M. Kaveh, M. Soumekh, and R. K. Mueller, "Tomographic imaging via wave equation inversion," *ICASSP 82,* May 1982, pp. 1553-1556.

[Opp75] A. V. Oppenheim and R. W. Schafer, *Digital Signal Processing,* Prentice-Hall, Englewood Cliffs, NJ, 1975.

[Pan83] S. X. Pan and A. C. Kak, "A computational study of reconstruction algorithms for diffraction tomography: Interpolation vs. filtered-backpropagation," *IEEE Transactions on Acoustics, Speech and Signal Processing,* October 1983, pp. 1262-1275.

[Sou84a] M. Soumekh, M. Kaveh, and R. K. Mueller, "Fourier domain reconstruction methods with application to diffraction tomography," *Acoustical Imaging,* Vol. 13, 1984, pp. 17-30.

[Sou84b] M. Soumekh and M. Kaveh, "Image reconstruction from frequency domain data on arbitrary contours," *International Conference on Acoustics, Speech and Signal Processing,* 1984, pp. 12A.2.1 - 12A.2.4.

[Sto80] Josef Stoer and Roland Bulirsch, *Introduction to Numerical Analysis,* Springer-Verlag, New York , 1980.